



Importance of catalyst stability *vis-à-vis* hydrogen peroxide formation rates in PEM fuel cell electrodes

Vijay A. Sethuraman^{a,1,2}, John W. Weidner^{a,*}, Andrew T. Haug^{b,3},
Marianne Pemberton^b, Lesia V. Protsailo^b

^a Center for Electrochemical Engineering, Department of Chemical Engineering, University of South Carolina, Columbia, SC 29208, USA

^b UTC Power, South Windsor, CT 06074, USA

ARTICLE INFO

Article history:

Received 30 January 2009

Received in revised form 23 April 2009

Accepted 24 April 2009

Available online 3 May 2009

Keywords:

Durability

Hydrogen peroxide

Oxygen reduction reaction

PEM fuel cell

Pt alloys

ABSTRACT

The role of catalyst stability on the adverse effects of hydrogen peroxide (H_2O_2) formation rates in a proton exchange membrane fuel cell (PEMFC) is investigated for Pt, Pt binary (PtX, X = Co, Ru, Rh, V, Ni) and ternary (PtCoX, X = Ir, Rh) catalysts supported on ketjen black (KB) carbon. The selectivity of these catalysts towards H_2O_2 formation in the oxygen reduction reaction (ORR) was measured on a rotating ring disc electrode. These measured values were used in conjunction with local oxygen and proton concentrations to estimate local H_2O_2 formation rates in a PEMFC anode and cathode. The effect of H_2O_2 formation rates on the most active and durable of these catalysts (PtCo and PtIrCo) on Nafion membrane durability was studied using a single-sided membrane electrode assembly (MEA) with a built-in reference electrode. Fluoride ion concentration in the effluent water was used as an indicator of the membrane degradation rate. PtIrCo had the least fluorine emission rate (FER) followed by PtCo/KB and Pt/KB. Though PtCo and PtIrCo show higher selectivity for H_2O_2 formation than unalloyed Pt, they did not contribute to membrane degradation. This result is explained in terms of catalyst stability as measured in potential cycling tests in liquid electrolyte as well as in a functional PEM fuel cell.

© 2009 Elsevier Ltd. All rights reserved.

1. Introduction

Electrochemical oxygen reduction reaction (ORR) on Pt in acid media occurs as a four-electron transfer reaction resulting in H_2O ($E^0 = 1.23$ V vs. SHE) and as a two-electron transfer reaction resulting in H_2O_2 ($E^0 = 0.695$ V vs. SHE) [1]. It is currently uncertain as to whether these two reactions occur in a parallel or in a serial fashion. The ratio of the extent of two-electron transfer reaction to that of the four-electron transfer reaction, the H_2O_2 selectivity, is a function of local water activity, and is typically between 0% and 20% for Pt [2]. The H_2O_2 selectivity is thought to have important consequences for PEM fuel cells from two perspectives—parasitic fuel loss as well as on the perceived role of H_2O_2 on membrane degradation [3–7]. As a result, almost all fuel cell catalyst groups study and report H_2O_2

selectivity as part of the characterization of novel fuel cell cathode catalysts.

The objective of this study is to evaluate the role of catalyst stability as well as the importance of H_2O_2 formation on Pt and Pt alloy catalysts. Both parasitic fuel losses due to H_2O_2 formation as well as its impact on durability are studied. In this article, the peroxide selectivity on binary and ternary Pt alloys during ORR is measured and the corresponding peroxide formation rates in a fuel cell anode and cathode are estimated. The most durable and active among the catalysts studied was evaluated in a single-sided MEA for their role in membrane degradation. The catalysts with the greatest selectivity for peroxide had the least membrane degradation and vice versa. This counter-intuitive result is explained in terms of their stability as measured in both liquid electrolyte cells as well as in an operating fuel cell.

2. Experimental

2.1. Catalyst synthesis

Binary and ternary Pt alloys supported on Ketjen Black (KB) high surface area carbon (EC300J Carbon black, Akzo Nobel Polymer Chemicals, Chicago, IL) with approximately 50% Pt loading were synthesized according to the wet chemistry procedure [8]. In

* Corresponding author at: Department of Chemical Engineering, Swearingen Engineering Center, University of South Carolina, 301 Main Street, Columbia, SC 29208, USA. Tel.: +1 803 777 3207; fax: +1 803 777 8265.

E-mail address: weidner@cec.sc.edu (J.W. Weidner).

¹ ISE Member.

² Present address: Environmental Energy Technology Division, Lawrence Berkeley National Laboratory, Berkeley, CA 94720, USA.

³ Present address: 3M Center, 3M Fuel Center Components, St. Paul, MN 55144, USA.

short, 2 g Ketjen Black powder as a carbon support was dispersed in deionized (DI) water, 5.75 g chloroplatinic acid ($\text{H}_2\text{PtCl}_6 \cdot 6\text{H}_2\text{O}$, Alfa Aesar) as a platinum salt was added to the dispersion and 5 ml 37% formaldehyde (HCOH, Aldrich Chemicals) as a reducing agent was introduced afterward. In order to control the platinum particle size [9], carbon monoxide (20% CO in N_2 , Praxair) was flowed to the dispersion when Pt was deposited on carbon. After being filtered, washed with DI water and dried in a vacuum oven at 90°C , the Pt/C catalyst precursor was re-dispersed in a known quantity of the precursor solution according to the element needed to be alloyed (for example, Cobalt nitrate solution ($\text{Co}(\text{NO}_3)_2 \cdot 6\text{H}_2\text{O}$ for Co), and the mixture was dried at 90°C . The dried mixture of Pt/C and the precursor compound was then heat-treated at 900°C for 1 h under a continuous flow of Argon (99.9%, Praxair). This step was to reduce metal ion to the corresponding metal by carbo-thermal reduction [8] and to alloy the Pt and the metal. This procedure is repeated with a corresponding precursor compound for synthesis of the ternary alloy. Detailed description of the synthesis can be obtained from [8] and [9]. Characterization of all of these binary and ternary alloys is carried out from a stability standpoint in this study.

All the catalysts reported in the remainder of this study are supported on Ketjen Black carbon ($\text{BET} = 800 \text{ m}^2 \text{ g}^{-1}$), unless noted otherwise. Pt/KB catalysts were synthesized in house and compared to two commercially available catalysts (Pt/KB and Pt/Vulcan XC-72R). The in-house Pt/KB catalyst performed as well as the commercially available ones and therefore the synthesized binary and ternary alloys were compared to commercially available Pt (TEC10E50E 46.7% Pt on Ketjen Black carbon, Tanaka Kikinokogyo KK, Japan) catalyst.

2.2. Rotating ring disc electrode (RRDE)

The binary and ternary Pt alloys were evaluated for their selectivity towards H_2O_2 formation using the rotating ring disc electrode technique. Catalyst coated glassy carbon electrodes were prepared as described by Schmidt et al. [10]. Aqueous suspensions of $1 \text{ mg catalyst ml}^{-1}$ were obtained by pulse-sonicating 20 mg of the catalyst with 20 ml triple-distilled, ultrapure water (Millipore Corporation) in an ice bath (70% duty cycle, 60 W, 15 min). Sonication was done using a Braun-Sonic U Type 853973/1 sonicator. A glassy carbon disc served as the substrate for the supported catalyst and was polished to a mirror finish ($0.05 \mu\text{m}$ deagglomerated alumina, Buehler®) prior to catalyst coating. An aliquot of calculated amount of catalyst suspension was pipetted onto the carbon substrate, which corresponded to a Pt loading of $\sim 14.1 \mu\text{g Pt cm}^{-2}$. After evaporation of water for 30 min in N_2 atmosphere (15 in-Hg, vacuum), $14 \mu\text{l}$ of diluted Nafion solution (5% aqueous solution, 1100 EW; Soluton Technology Inc., Mendenhall, PA) was pipetted on the electrode surface and further evaporated for 30 min in N_2 atmosphere (15 in-Hg, vacuum). Nafion® was used to adhere the Pt/Vulcan particles onto the glassy carbon electrode (the ratio of $\text{H}_2\text{O}/\text{Nafion}^\circledast$ solution used was ca. 100/1). Previous work by Paulus et al. indicate that this procedure yielded a Nafion® film thickness of ca. $0.1 \mu\text{m}$ and that the utilization of the Pt/Vulcan catalyst (based on H-adsorption charge) on the electrode with this film was $\sim 100\%$. In addition, the Nafion film rejects anions and only transports protons to the catalyst surface. It thus plays a role in minimizing anion adsorption on to the catalyst.

The catalyst-Nafion® coated electrode was immersed in deaerated (UHP Nitrogen, Praxair) Perchloric acid (HClO_4 , 70%, ULTREX II® Ultrapure Reagent Grade, J. T. Baker) of varying concentrations for further synchronized chrono-amperometric and potentiodynamic experiments. Though a variety of supporting electrolytes are reported in the literature, anion adsorption on Pt is minimal for only a few electrolytes [11] (e.g., trifluoromethane sulfonic acid (TFMSA) and HClO_4). In addition, the ultrapure reagent grade HClO_4 used in

this study is free of ionic impurities; especially since Cl^- ions, even in trace amounts (i.e. 1 ppm), is shown to drastically change both the activity and the reaction pathway of ORR on Pt catalysts [11–13]. All RRDE experiments were performed at atmospheric pressure and all solutions were prepared from ultrapure water (Millipore Inc., $18.2 \text{ M}\Omega \text{ cm}$).

The electrochemical measurements were conducted in a standard electrochemical cell (RDE Cell®, Pine Instrument Company, NC) immersed in a custom-made jacketed vessel, temperature of which was controlled by a refrigerated/heating circulator (Julabo Labortechnik GMBH). A ring-disk electrode setup with a bi-potentiostat (Bi-Stat®, Princeton Applied Research Inc., TN) in conjunction with rotation-control equipment (Pine Instrument Company, NC), EC-Lab® software (version 8.60, Bio-logic Science Instruments, France) was used to control the bi-potentiostat. The Pt ring electrode was held at 1.2 V vs. SHE where the oxidation of peroxide is diffusion limited. The catalyst coated glassy carbon disc electrode (5 mm diameter, 0.1966 cm^2 area, DT21 Series, Pine Instrument Company, NC) was scanned between 0 and 1.2 V vs. SHE to characterize H_2O_2 formation within the potential range relevant to fuel cell operating conditions. Potentials were determined using a mercury-mercurous sulfate ($\text{Hg}/\text{Hg}_2\text{SO}_4$) reference electrode. All potentials in this study, however, refer to that of the standard hydrogen electrode (SHE). A high-surface area Pt cylindrical-mesh (5 mm diameter, 50 mm length) attached to a Pt wire (0.5 mm thick, 5 mm length) was used as the counter electrode.

2.2.1. Effect of oxygen concentration

The effect of oxygen concentration on ORR and H_2O_2 formation kinetics on Pt electrode was studied by varying the concentration of oxygen in the solution. The following three gases were used: oxygen (UHP grade, Praxair), Air (Industrial, Praxair) and 10.01% oxygen in nitrogen (Airgas). A gas flow meter (0–500 ml range, Dwyer Instruments Inc., IN) was used to control the flow of the gas feed at $\sim 100 \text{ ml min}^{-1}$ into the electrolyte. The electrochemical cell was sealed during the experiments to keep air from affecting the concentration of dissolved oxygen in the electrolyte. The concentration of dissolved oxygen in the electrolyte was estimated using the solubility values for oxygen in pure liquid water at 25°C and 101 kPa [14].

2.2.2. Effect of pH

The effect of proton concentration on ORR and H_2O_2 formation kinetics on Pt, PtCo and PtIrCo catalysts was studied by varying the acidity of HClO_4 in the 2.0–0.1 M concentration window (~ -0.301 to 1 pH, assuming $K_a \gg 1$ for HClO_4). Between solution changes, the electrochemical cell and its components were washed and boiled in DI water for 5 h to ensure accurate pH levels. The catalyst-Nafion® coated electrode was also cleaned in a sonicator before every experiment with triple distilled ultrapure water.

2.2.3. Collection efficiency

Standard procedure [15] for the determination of collection efficiency of a ring-disk electrode was followed. The electrodes were prepared as described above. The experiment was carried out in an electrochemical cell in deaerated (UHP Nitrogen, Praxair) 0.1 M H_2SO_4 (96.5%, J.T. Baker) with 10 mmol l^{-1} $\text{K}_3\text{Fe}(\text{CN})_6$ (99.7%, J.T. Baker). The disk electrode was swept at 1 mV s^{-1} [vs. SHE] while the Pt ring was held at a constant potential of 1.2 V [vs. SHE]. At this ring potential, the oxidation of $[\text{Fe}(\text{CN})_6]^{4-}$, produced at the disk electrode, to $[\text{Fe}(\text{CN})_6]^{3-}$, proceeds under pure diffusion control. The collection efficiency was determined as $N = I_{\text{ring}}/I_{\text{disk}} = 0.20$, which was independent of disk potential and consistent with the theoretical collection efficiency provided by the manufacturer of the ring-disk electrode [16].

2.3. Potential cycling—RDE cell

Potential cycling between 0.65 and 1.2 V vs. SHE was carried out in a standard RDE electrochemical cell at 25 °C and 1 atm in either 0.1 M H₂SO₄ or 0.1 M HClO₄. A high-surface area Pt cylindrical-mesh (5 mm diameter, 50 mm length) attached to a Pt wire (0.5 mm thick, 5 mm length) was used as the counter electrode. Platinized Pt electrode in contact with H₂ gas acted as the reference electrode. The electrode was held at each vertex potential for 5 s for a total of 20,000 cycles. Electrochemical surface area measurements were conducted every 1000 cycles. A potentiostat (Princeton Applied Research Model 273A, Oak Ridge, TN) in conjunction with the Corware software (Scribner Associates Inc., Southern Pines, NC) was used for these measurements.

2.4. Electrochemical surface area (ECA) measurements

2.4.1. RDE cell

Cyclic voltammograms (CV) on the thin film RDE were recorded between 0 and 1.2 V vs. SHE at 25 °C in deaerated 0.1 M H₂SO₄. The starting potential was the open circuit potential and scan rate was 5 mV s⁻¹. A typical CV consisted of three to five cycles, and showed very little cycle-to-cycle variation after the first cycle. For each catalyst studied, the CVs were recorded initially and after every 1000 cycles during the potential cycling test. The ECA was calculated from the charge under the voltammetric peaks corresponding to H₂ adsorption region in the CV after correcting for double layer charging (i.e., capacitive component) [17]. Mathematically, the ECA is given as

$$ECA = \frac{Q_{Pt-H}}{QW} \quad (1)$$

In this equation, W corresponds to Pt loading in the catalyst layer in mg_{Pt} cm⁻² (geometric area) and \bar{Q} , the charge density which is taken to be 210 μC cm⁻² (real area). This charge density corresponds to that of the Pt (1 0 0) facet [18,19]. We assume this charge density to be valid for all the catalysts studied in this work. Finally, Q_{Pt-H} , the charge corresponding to H₂ adsorption, is calculated from

$$Q_{Pt-H} = \frac{1}{v} \left(\int_{V_1}^{V_2} I dV - I_{dl} \Delta V \right) \quad (2)$$

The accuracy of this estimation depends on the identification of V_1 and V_2 in the CV, which are respectively, the potential where H adsorption begins and the potential where H coverage is complete before the rate of hydrogen evolution becomes significant. The term $I_{dl} \Delta V$ represents the double layer capacitance between these two potentials.

2.4.2. Fuel cell

The CVs were recorded on the cathode after the cathode gas (N₂) was replaced with liquid water and the anode gas (pure H₂) was replaced with 4% H₂ in N₂. The CV parameters were similar to that of the RDE cell except the upper potential was 1 V. The ECA was estimated according to the above procedure.

2.5. Single-sided membrane electrode assembly with a reference electrode

The effect of Pt alloy catalysts on membrane durability was studied using single-sided MEAs designed with built-in reference electrodes. In order to specify the potential of the working electrode (anode or cathode), a reference electrode was placed inside the membrane in such a way that it was electronically isolated from the anode and the cathode but was in contact with H₂ gas. Since it

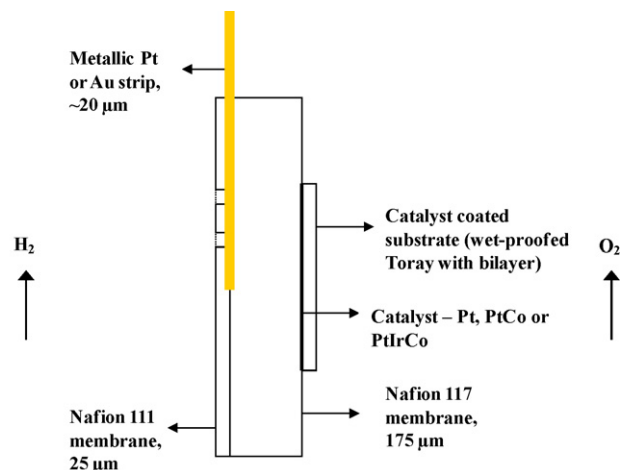


Fig. 1. Schematic of a single-sided MEA with reference electrode. H₂ was fed on one side while O₂ was fed on the other. The O₂ side had the catalyst (Pt, PtCo or PtIrCo) and was subjected to a fixed potential of 0.6 V vs. the H₂ on Au reference electrode. The reference electrode was electronically isolated from the flow-field by a thin Nafion® 111 membrane.

is impossible to place a Pt or Au foil or wire inside a thin membrane, the reference electrode was sandwiched between two membranes. A perforated thinner membrane (Nafion® 111, in this case) electronically insulated the reference electrode from the anode Fig. 1 shows the design of such an electrode. The working membrane in this case was thicker Nafion 117® membrane. For the reference electrode to work in a regular (two-sided) MEA, the flow-field should have an additional channel outside the projected electrode area so that the reference electrode has access to H₂. The same design as described above was used with electrode on only one side of the MEA. This design was an improvement over earlier durability experiments with single-sided MEA reported by Mittal et al. [20–23]. In that, they built single-sided MEAs (MEAs with catalysts and substrate on one side and no catalyst or substrate on the other side) they measured the fluorine emission rates at open circuit conditions. Their test matrix comprised of four such configurations with hydrogen and oxygen flowing on the anode and the cathode respectively and nitrogen flowing on either electrodes. In this work, with the inclusion of the reference electrode, a potential can be applied upon the single-sided electrode configuration. The effect of potential on membrane durability can now be studied. The effect of Pt, PtCo and PtIrCo catalysts on membrane degradation was studied at 0.6 V vs. SHE using these single-sided MEA setup with reference electrode.

2.5.1. Fluorine emission rates (FER)

Effluent water samples from the single-sided electrode experiment were collected in polyethylene bottles and analyzed for the presence and concentration of fluoride ions using a Dionex ICS-200 ion chromatography system. In addition to this, a colorimetric method (Chemeterics Inc., VA) was used to measure the concentration of H₂O₂ in the effluent water.

2.6. Fuel cell construction

The PtCo, PtIrCo synthesized in house as well as commercially available Pt/C catalyst (TEC10E50E 46.7% Pt on Ketjen Black carbon [BET = 800 m² g⁻¹], Tanaka Kikinokogyo KK, Japan) were each mixed with Nafion® (5% aqueous solution, 1100 EW; Solution Technology Inc., Mendenhall, PA) ionomer and the resulting catalyst-ionomer ink (79% catalyst, 21% Nafion®) was coated onto Teflon® based (EI DuPont de Nemours & Company) decals. These catalyst-coated decals were dried in N₂ at room temperature

and atmospheric pressure for 30 min. Catalyst-coated membranes (CCMs), 6.5 cm × 6.5 cm, were then made by hot pressing the catalyst-coated Teflon® decals onto both sides of Nafion® 112 membranes (proton form) at 130 °C and 4500 lbs for 300 s. Reinforced silicon, un-reinforced silicon and Teflon® pads were used as supports for this process. While one side of the CCMs always had Pt catalyst, the other side had Pt, PtCo or PtIrCo catalyst. The Pt, PtCo, and PtIrCo CCMs had similar Pt loadings of ~0.4 mg_{Pt} cm⁻² on both the anode and the cathode sides.

The CCMs were each assembled into a fuel cell (25 cm² hardware, Fuel Cell Technologies Inc., NM). Wet-proofed Toray® paper with micro-porous layer (243 μm total; Toray Industries, Japan) was used as gas diffusion media (GDM). Gaskets were chosen in such a way that they allowed for 21% compression on the GDMs at 30 in-lbs of torque on the bolts. The fuel cell had non-porous modular serpentine flow channels on the anode side and interdigitated flow channels (IDFF) on the cathode side. The assembled fuel cell was tested for throughput, gas crossover and overboard leaks and then conditioned with H₂/O₂ (anode/cathode) in a fuel cell test stand (Habco Inc., CT) at 80 °C and 101 kPa (absolute). Several current–voltage (VI) curves were measured in hydrogen and oxygen with 30% and 25% utilizations respectively until a steady high performance was reached.

2.7. Potential cycling—fuel cell

Once the fuel cell reached a steady performance, the cathode gas was switched to N₂ and the temperatures on the humidity bottles were lowered such that the relative humidity was 50%. The cell temperature was increased to 120 °C and the cathode potential was cycled between 0.87 and 1.05 V vs. SHE. The cathode remained at each potential for 1 min each. The upper potential was lowered from 1.2 V (as was the case for the potential cycling in the RDE cell at 25 °C) to 1.05 V vs. SHE to avoid carbon corrosion, which could occur at 120 °C at higher potentials. The potential cycling in the absence of O₂ captures the stability of the cathode catalyst whereas the potential hold experiment on the single-sided MEA captures the isolated effect of cathode peroxide formation on membrane durability. Electrochemical area (ECA) measurements were conducted at routine intervals. The ECA measurements on the cathode were done after replacing N₂ with liquid water. In addition to ECA measurements, performance curves were recorded with H₂/Air and H₂/O₂ at regular intervals. After 2800 cycles, the fuel cells were dismantled and XRD and EMPA analysis were done on the MEAs. X-ray diffraction data was used to analyze phase separation, crystal structure and particle size changes. Electron probe microanalysis was done to map the concentration of elements (i.e., Pt, Co or Ir) in the membrane.

2.8. Fenton tests

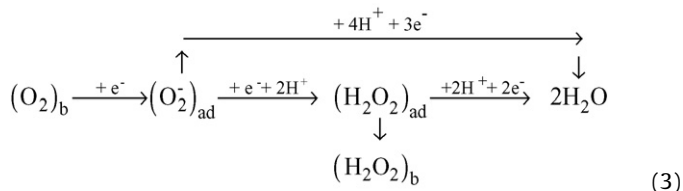
Nafion® 111 membrane (H⁺ form, DuPont Fluoroproducts, NC) samples measuring ~2 in. × 2 in. were cut and heated in clean glass vials containing water at 80 °C for 2 h to remove any surface impurities and solvents. The water was later drained from the vials and the membrane was dried in vacuum at 80 °C for 4 h. The dry weight of the membrane was then measured. This weight was used to prepare various concentrations of aqueous ferrous sulfate (FeSO₄·7H₂O, 98.1% assay, Fischer Scientific Company, NJ) and cobalt nitrate (Co[NO₃]₂·6H₂O, reagent grade, Fischer Scientific Company, NJ) solutions such that the respective Fenton ion (Fe²⁺ and Co²⁺) uptake would vary. The dried Nafion® membrane was placed in these solutions for 15 h in a N₂ atmosphere. This process impregnated various amounts of Fe²⁺ and Co²⁺ ions into the membrane samples. After this impregnation process, the membrane was dried in vacuum at 80 °C for 4 h. The dry weight

of the membrane impregnated with the Fenton ions was then measured.

The Fenton ion impregnated membrane samples were each placed in a Teflon® container containing 100 ml of 3% hydrogen peroxide aqueous solution (30%, VWR International) at 80 °C. Oxygen radicals are produced by the Fenton reaction, where the major step is H₂O₂ + M²⁺ → M³⁺ + HO• + HO⁻, where Mⁿ⁺ represents a metal ion. The radical species attack the membrane via H abstraction, HO• + RH → H₂O + R• [3]. The radical R can further react to produce peroxy and hydroperoxy radical triggering a cascade of degradation reactions. Since hydrogen peroxide decomposes in the presence of a metal ion, the solution was replaced once every 24 h and the leachate was saved for fluorine analysis. After 96 h, the membrane was dried in vacuum at 80 °C for 4 h. The weight loss, if any was recorded. The leachate was analyzed for fluorine using a Dionex ICS-200 ion chromatography system.

3. Theory

The ORR on Pt electrode occurs via the following reaction scheme:



It is currently uncertain whether the first electron transfer precedes the adsorption of O₂ or the adsorption of O₂ and the first electron transfer occur simultaneously. Nevertheless, the rate determining step appears to be the addition of the first electron to oxygen [24]. The second uncertainty is whether the splitting of the O–O bond occurs before the formation of the reaction intermediates (the direct 4e⁻ pathway) or whether the superoxo radicals react with the surrounding protons to form H₂O₂, which is further reduced to H₂O (the serial 4e⁻ pathway) or escapes into the bulk.

The two-electron transfer reaction of O₂ reduction to H₂O₂, captured by the Pt ring, was analyzed in this study. At the ring, the H₂O₂ produced at the disk is oxidized back to O₂. The fraction of H₂O₂ formation, $\chi_{\text{H}_2\text{O}_2}$, can be determined from the collection efficiency, ring and disk currents by the expression

$$\chi_{\text{H}_2\text{O}_2} = \frac{2I_{\text{ring}}/N}{I_{\text{disk}} + I_{\text{ring}}/N} \quad (4)$$

The measured current density j corresponding to H₂O₂ formation on a film covered RDE for the first-order ORR kinetics was previously reported to take the following expression [25], in terms of kinetic and mass-transport dependent currents

$$\frac{1}{j} = \frac{1}{j_{\text{kin}}} + \frac{\delta_f}{nFD_{\text{O}_2}^f C_{\text{O}_2}^f} + \frac{1}{j_D} \quad (5)$$

where j is

$$j = \frac{I_{\text{ring}}}{NA} \quad (6)$$

j_{kin} is the current density in the absence of mass transfer effects and j_D is the diffusion current given by the Levich equation.

$$j_D = 0.62nFD_{\text{O}_2}^{2/3} C_{\text{O}_2}^* \nu^{-1/6} \omega^{1/2} \quad (7)$$

The concentration of O₂ in the solution was calculated from the partial pressure of O₂ in the inlet gas and O₂ solubility data for pure liquid water at corresponding temperature and 101 kPa [14]. The difference in O₂ solubility in pure liquid water and in HClO₄ (up to

2 M) was assumed to be negligible. Combining Eqs. (5) and (7) and solving for j_{kin} gives

$$j_{\text{kin}} = \frac{jnFD_{\text{O}_2}^f C_{\text{O}_2}^f D_{\text{O}_2}^{*2/3} C_{\text{O}_2}^* \omega^{1/2}}{nFD_{\text{O}_2}^f C_{\text{O}_2}^f D_{\text{O}_2}^{*2/3} C_{\text{O}_2}^* \omega^{1/2} - \delta_{\text{H}} j D_{\text{O}_2}^{*2/3} C_{\text{O}_2}^* \omega^{1/2} - 1.6v^{1/6} j D_{\text{O}_2}^f C_{\text{O}_2}^f} \quad (8)$$

The purely kinetic portion of the H_2O_2 formation rate is

$$R_{\text{H}_2\text{O}_2} = \frac{j_{\text{kin}}}{2F} = k_f(C_{\text{O}_2})^a(C_{\text{H}^+})^b \quad (9)$$

where

$$k_f = k_f^0 \exp\left[\frac{\alpha F \eta}{RT}\right] \quad (10)$$

In Eq. (9), a and b are reaction orders with respect to O_2 and H^+ respectively. Only the forward rate term is used in Eq. (9) because at 0.6 V vs. SHE and below, the rate of oxidation of H_2O_2 to O_2 is negligible. The kinetic rate constant k_f was estimated for different potentials by plotting H_2O_2 production rate as a function of oxygen concentration for various potentials. Since the electrode reaction rate was earlier shown by Damjanovic and Hudson [26] to be faster on an oxide-free Pt surface than on an oxide-covered surface, both the forward and the reverse scans were used to estimate the reaction rate constant. The upper and lower bounds for the rate constants would therefore correspond to oxide-free and oxide-covered Pt surfaces respectively. The potential dependence of this rate constant is given in Eq. (10).

The activation energies for hydrogen peroxide formation reaction were evaluated by using the Arrhenius equation [27]:

$$k_f^0 = k_{f,0}^0 \exp\left[\frac{E_a}{RT}\right] \quad (11)$$

This procedure is analogous to those described by Neyerlin et al. [28] and Bard and Faulkner [29]. The activation energies for H_2O_2 formation on supported Pt catalysts were compared to the computationally estimated activation energies reported in the literature. For example, using density functional theory (DFT), Anderson and Albu [30], Sidik and Anderson [31] and Wang and Balbuena [32] have reported activation energies for H_2O_2 formation on Pt₁, Pt₂ and Pt₃ sites respectively.

4. Results and discussion

4.1. H_2O_2 selectivity, activity and stability of binary and ternary Pt alloys

The selectivity towards H_2O_2 formation for binary (PtX, X = Co, Rh, Ru, Ni and V) and ternary (PtCoX, X = Ir, Rh) alloy catalysts supported on high surface area Ketjen Black carbon are shown in Figs. 2a and 3a and respectively. The polarization curves for ORR on these binary and ternary alloys are shown in Figs. 2b and 3b respectively. Data corresponding to the negative potential sweep (i.e., starting from 1.2 V vs. SHE and scanning towards 0 V vs. SHE) are shown in these figures. Fig. 2a shows the selectivity of binary alloys compared to Pt. The selectivity values in the neighborhood of 0.6 V vs. SHE and at 0 V vs. SHE are of interest because of their relevance to fuel cell operating conditions. Normally, fuel cell cathode potentials are higher than the equilibrium potential for H_2O_2 formation (i.e., 0.695 V vs. SHE) except under very high load conditions when the local cathode potential could go negative of 0.695 V vs. SHE. On the anode, the local potential is close to the reversible hydrogen electrode potential. In general, the binary and ternary alloy catalysts show higher selectivity towards H_2O_2 formation than Pt. The PtRu catalyst is the only exception, which shows the least selectivity of these catalysts. As shown in Fig. 2b, the disc current

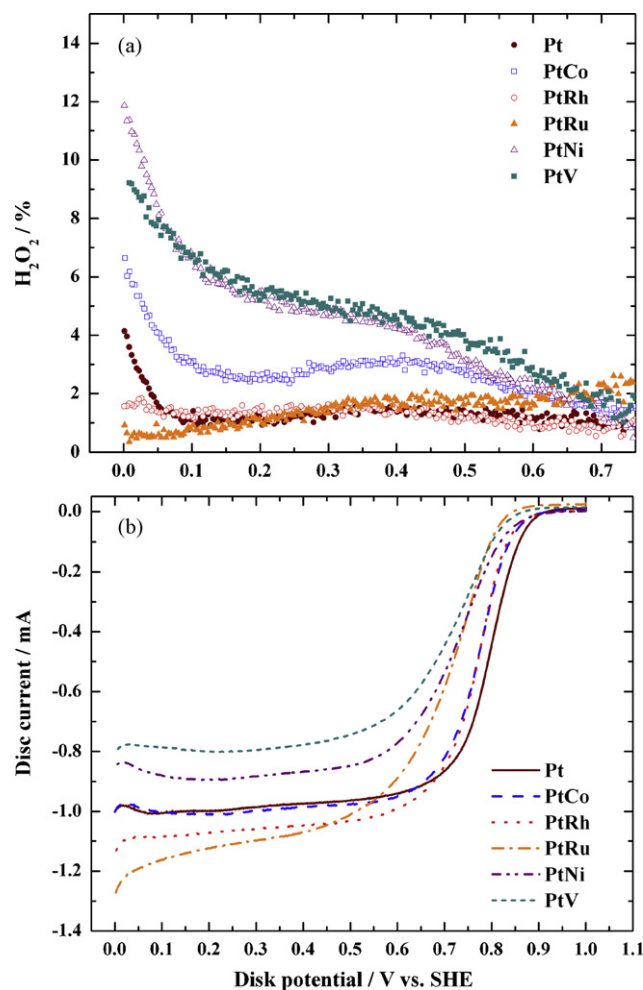


Fig. 2. (a) % H_2O_2 formed during the ORR on binary alloy catalysts PtCo (□), PtRh (○), PtRu (△), PtNi (●), PtV (■) compared to Pt (●). (b) Polarization curves for the ORR on binary alloy catalysts PtCo (dash), PtRh (dot), PtRu (dash dot), PtNi (dash dot dot), PtV (short dash) compared to Pt (line). The thin film RRDE (2500 rpm) experiments were done in 1 M HClO_4 solution (pH -0.3) bubbled with pure O_2 at 25 °C and 1 atm.

corresponding to PtRu does not show a characteristic point of inflexion near 0 V vs. SHE evident for all the other catalysts. The ring current (and thus the H_2O_2 selectivity), starts around 0.7 V vs. SHE for PtRu and reaches a maximum around 0.4 V vs. SHE and then decreases monotonically until 0 V vs. SHE. Stamenkovic et al. [33] also observed similar results for PtRu and it is unclear as to why at potentials lesser than 0.1 V vs. SHE, PtRu is a better peroxide catalyst (i.e., lower peroxide selectivity) than pure Pt and most other binary and ternary Pt alloys. Clearly, in addition to Pt atoms Ru atoms are also involved in the cleaving of the O–O bond. For ORR on a pure Ru electrode in acid solution, see [34].

Among the binary alloys studied, PtNi shows the highest selectivity towards H_2O_2 formation followed by PtV and PtCo. Comparison of H_2O_2 selectivity of ternary alloys with Pt and PtCo is presented in Fig. 3a. The stability of these binary and ternary alloy catalysts was evaluated by potential cycling experiments in an RDE cell. The results are summarized in Fig. 4. The respective lattice constant for Pt is shown above each catalyst in Fig. 5 and a trend can be seen where the catalyst with lower lattice constant shows better stability. The averaged crystallite size obtained via XRD for commercial Pt (TEC10E50E) and freshly synthesized PtRh, PtCo, PtIrCo and PtRhCo were 33, 31, 62, 59 and 35 Å, respectively. The true electrochemical area (ECA) corresponding to the charge under the voltammetric peaks for hydrogen adsorption, corrected for dou-

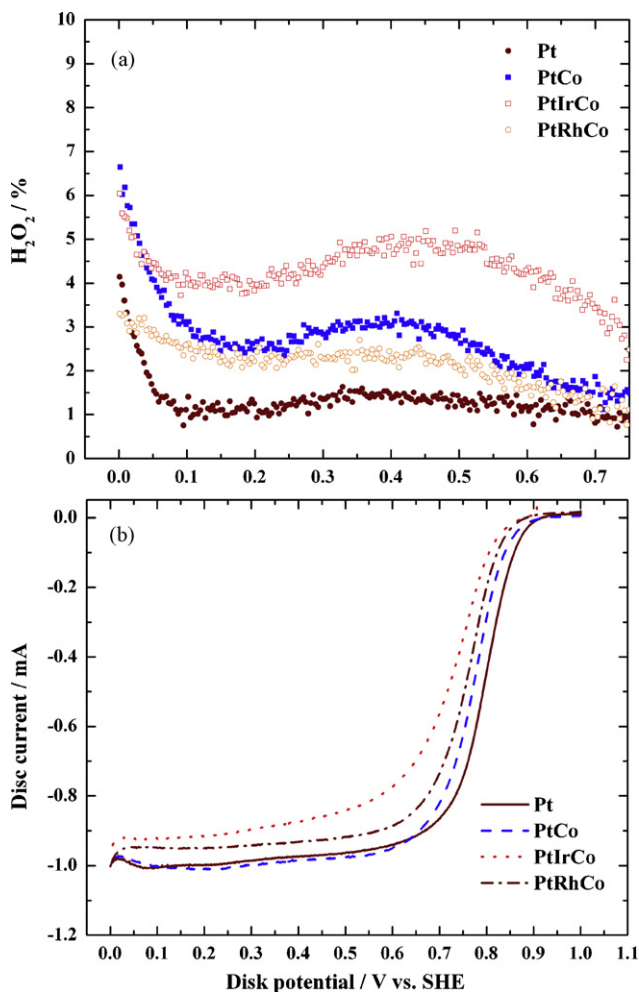


Fig. 3. (a) % H₂O₂ formed during the ORR on ternary alloy catalysts PtIrCo (●) and PtRhCo (○) compared to Pt (■) and PtCo (□). (b) Polarization curves for the ORR on ternary alloy catalysts PtIrCo (dot), and PtRhCo (dash dot) compared to Pt/KB (line) and PtCo (dash). The thin film RRDE (2500 rpm) experiments were done in 1 M HClO₄ solution (pH ~0.3) bubbled with pure O₂ at 25 °C and 1 atm.

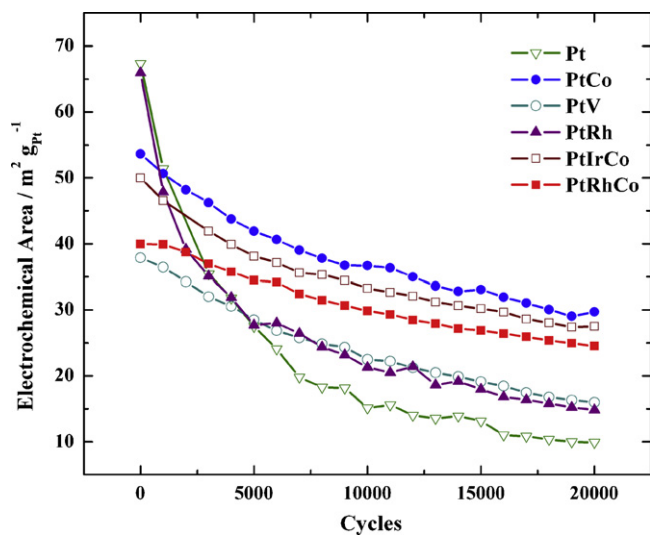


Fig. 4. Stability of binary and ternary Pt catalysts during cycling between 0.65 and 1.2 V vs. SHE in 0.1 M H₂SO₄ and at 25 °C. PtCo and PtIrCo, the most durable of these catalysts lost 44.58% and 44.94% of their initial electrochemical area respectively after 20,000 cycles. Pt lost 85.28% of its initial electrochemical area under similar conditions.

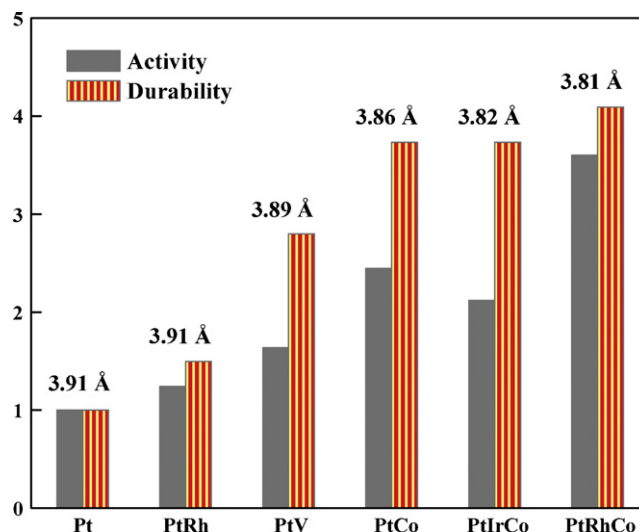


Fig. 5. Mass activity and durability of Pt binary and ternary catalysts supported on Ketjen black carbon relative to Pt. The durability reported here reflects the electrochemical area at the end of 20,000 cycles between 0.65 and 1.2 V (5 s each) in 0.1 M HClO₄ at 25 °C and 1 atm. The respective lattice constant value is shown above the bars for each catalyst.

ble layer charging, is shown for every 1000 cycles for up to 20,000 cycles. Qualitatively, all catalysts show ECA loss upon potential cycling. It can be seen that though Pt had the highest initial ECA, with ~85% of it lost after 20,000 cycles. PtCo, PtRhCo and PtIrCo were the most stable among these catalysts losing 44.58%, 38.6%, and 44.94% of their initial ECAs respectively. The activity and durability of these catalysts relative to Pt is shown in Fig. 5. Activity bars correspond to ratio of specific activity of a catalyst in terms of ORR current at 900 mV vs. SHE normalized to the ESA to that of Pt. Durability bars correspond to the ratio of ECA of a catalyst at the end of 20,000 cycles to that of Pt. PtCo, PtRhCo and PtIrCo show the best activity and durability among the catalysts studied.

4.2. H₂O₂ kinetics and formation rates in a PEMFC anode and cathode

The kinetics of electrochemical reduction of O₂ to H₂O₂ was studied in detail for PtCo and PtIrCo, the two catalysts that showed good initial specific activity and stability in the RDE tests. The rate constant, k_f , was measured from the kinetic portion of the ring current (Eq. (9)) for Pt, PtCo and PtIrCo and is shown in Fig. 6. It shows the potential dependence of the rate constants according to Eq. (10). The data between overpotential values 0–0.2, 0.2–0.45 and 0.45–0.6 V was fit with three separate linear equations. The resulting intercept, k_f^0 , for these catalysts is summarized in Table 1. Since k_f is a direct measure of the ring current, PtCo and PtIrCo show higher values than Pt.

The H₂O₂ formation rates measured as a function of water activity, potential and temperature using RRDE experiments was used to predict H₂O₂ formation rates at the anode and cathode of PEM fuel cell. Peroxide formation rate at the anode was predicted using oxygen permeability from the cathode and $\chi_{\text{H}_2\text{O}_2}$. Peroxide formation rate at the cathode was estimated via Eq. (9), i.e. as a product of the rate constant and the local reactant concentrations. Peroxide formation at the cathode occurs only for fuel cells operating under considerable load (i.e., high cell current) such that the local potential goes negative relative to the equilibrium potential for peroxide formation. For estimation of cathode peroxide rates, local potential at the cathode was taken to be 0.6 V (i.e., $\eta = 0.095$ V).

Nafion® is a super-acid catalyst and hence the local acidity at the catalyst-membrane interfaces was calculated from the local

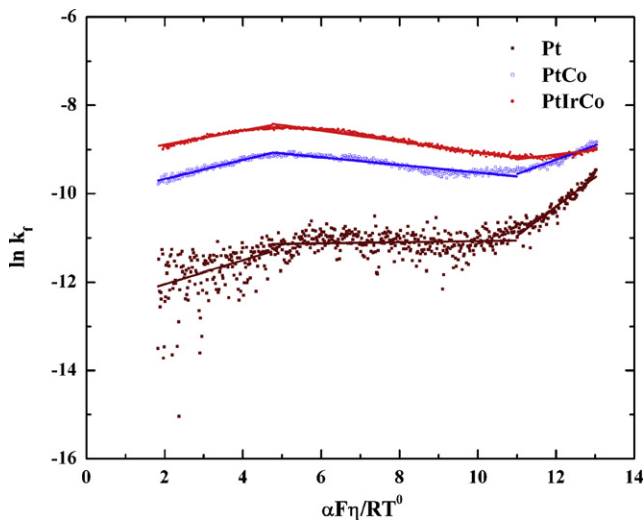


Fig. 6. Electrochemical rate constant for H_2O_2 formation, k_f , as a function of overpotential, $\eta = E_{\text{app}} - E^0$, $E^0 = 0.695$ V vs. SHE, for Pt, PtCo and PtIrCo catalysts supported on Ketjen black carbon. The data between η values 0–0.2 V, 0.2–0.45 and 0.45–0.6 V was fit with three separate linear equations (shown as lines). The value of $\alpha = 0.05$, $T^0 = 25^\circ\text{C}$. Data was obtained in 1 M HClO_4 bubbled with pure O_2 at 1 atm.

water content and the fixed number of sulfonic acid groups. The water sorption properties of Nafion[®] as a function of temperature and water activity had been studied by several laboratories [35–40]. Using a novel tapered element oscillating microbalance (TEOM) technique, Jalani et al. [37] measured water uptake in Nafion as a function of water activity in vapor phase between 30°C and 110°C and reported that the water uptake increased with temperature and was highest at 110°C . The difference in water uptake between 30°C and 110°C is negligible for lower water activities ($a_w < 0.7$). This is reported by Jalani et al. (experimental) and discussed in detail by Motupally et al. (simulations) [41]. For this work, the absorption isotherm of Nafion[®] 117 membranes measured at 30°C by Zawodzinski et al. [38] were used. Between water activity values of 0 and 1, the experimentally measured absorption isotherm was fit to the following polynomial [42]:

$$\lambda = 0.043 + 17.81[a_w] - 39.85[a_w]^2 + 36.0[a_w]^3 \quad (12)$$

In this equation, λ represents the number of water molecules per sulfonic acid group in the polymer and a_w represents the activity of water, which is the effective mole fraction of water given by p_0/p^* ,

where p^* is the vapor pressure of water, in bar. p^* was calculated from the Antoine correlation:

$$\ln p^* = A_1 - \frac{B_1}{T + C_1} \quad (13)$$

The constants are $A_1 = 11.6832$, $B_1 = 3816.44$, $C_1 = -46.13$ [43]. Inside a fuel cell, this water activity is essentially the equilibrium relative humidity expressed as a fraction. The concentrations of H_2O and H^+ in the polymer are respectively expressed as

$$C_{\text{H}_2\text{O}} = \frac{\rho\lambda}{\text{EW}} \quad (14)$$

$$C_{\text{H}^+} = \frac{C_{\text{H}_2\text{O}}}{\lambda} \quad (15)$$

In these equations, EW is the equivalent weight of the polymer (taken to be 1100) and ρ is the humidity-dependent density of the polymer given by

$$\rho = \frac{1.98 + 0.0324\lambda}{1 + 0.0648\lambda} \quad (16)$$

It was assumed that all sulfonic acid groups exist in a completely dissociated form. Relating MEA acidity to water activity and hence to the humidity of the incoming gases facilitates in computing peroxide rates inside a fuel cell. Quantitatively, the measured peroxide rates via the RRDE experiments at a particular oxygen concentration, pH value and temperature should equal the peroxide rates inside the fuel cell at same pH value and temperature. Activation energies for H_2O_2 formation on supported Pt catalysts were estimated from kinetic currents obtained at 15°C , 25°C , 35°C and 45°C . Oxygen permeability through Nafion[®] depends greatly on the water content of the membrane. It has been shown by Sakai et al. [44] that O_2 diffusion rates in a completely dry Nafion[®] membrane has values similar to that in PTFE and approaches the limit of liquid water with increasing water content. O_2 permeability was estimated using electrochemical monitoring technique (EMT) as a function of humidity and temperature and is comparable to those estimated by gas chromatography (GC) method [45]. Between 25% and 100% relative humidity of the feed gas, the permeabilities differ by as much as an order of magnitude. Permeability for other temperatures and water contents were estimated by the following equation which was derived by fitting the measured permeability values:

$$P_{\text{O}_2}^m = (1.002 \times 10^{-14} - 9.985 \times 10^{-15} a_w) \times \exp[(0.0127 + 2.3467 \times 10^{-2} a_w)T] \quad (17)$$

Table 1

Average H_2O_2 selectivity and formation rates on supported Pt, binary and ternary Pt fuel cell catalysts. H_2O_2 selectivity and formation rates were respectively calculated according to Eqs. (1) and (2). High surface area Ketjen Black carbon ($\text{BET} \sim 800 \text{ m}^2 \text{ g}^{-1}$) was the support for all the catalysts unless noted otherwise.

Catalyst	% H_2O_2 at		k_f^0 ($\times 10^5 \text{ mol}^2 \text{ cm}^{-5} \text{ s}^{-1}$)			H_2O_2 formation rates ^d ($\text{mol cm}^{-2} \text{ s}^{-1}$)	
	0.6 V vs. SHE	0.025 V vs. SHE	0–0.2 V vs. SHE	0.2–0.45 V vs. SHE	0.45–0.6 V vs. SHE	Anode ^b ($\times 10^{12}$)	Cathode ^c ($\times 10^6$)
Pt	0.75	2.78	1.87	2.73	2.56	0.342	0.007
Pt ^a	0.69	5.5	1.74	2.94	1.05	0.674	0.004
PtCo	2.11	5.36	1.34	14.36	4.17	0.657	0.017
PtCo ^a	3.65	8.4	1.84	1.78	5.21	1.031	0.022
PtNi	2.53	10.62	2.76	14.99	3.39	1.302	0.014
PtRh	0.74	1.28	2.465	5.15	1.25	0.157	0.005
PtRu	1.85	0.55	45.10	13.53	4.06	0.067	0.017
PtV	2.99	8.65	3.91	10.45	3.98	1.061	0.016
PtIrCo	5.39	5.05	6.17	27.18	9.28	0.338	0.018
PtRhCo	2.09	2.76	2.21	14.48	4.37	0.618	0.038

^a Supported on Vulcan XC-72R.

^b Evaluated at local potential at the anode was assumed to be 0 V vs. SHE, which translates to an overpotential of 0.695 V for H_2O_2 formation

^c Local potential at the anode was assumed to be 0.6 V vs. SHE, which translates to an overpotential of 0.095 V for H_2O_2 formation

^d H_2O_2 rates were estimated at 75°C , 1 atm and 94% RH conditions. Measured activation energies corresponding to H_2O_2 formation on supported Pt catalyst was used to estimate H_2O_2 rates at 75°C for all supported Pt binary and ternary alloys catalysts.

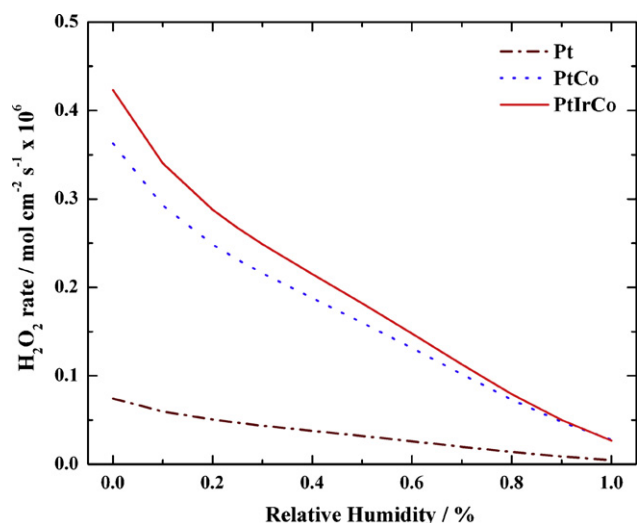


Fig. 7. Estimated rates of H_2O_2 formation/mol $\text{cm}^{-2} \text{s}^{-1}$ in the cathode side of a PEM fuel cell for Pt (dash dot), PtCo (dot) and PtIrCo (line) catalysts as a function of relative humidity at 75°C . Local potential at the cathode was assumed to be $\sim 0.6 \text{ V}$ vs. SHE, which translates to an overpotential of 0.095 V for H_2O_2 formation.

Oxygen solubility at the membrane-cathode catalyst layer interface, $C_{\text{O}_2}^c$, was estimated using the following relation:

$$C_{\text{O}_2}^c = \frac{P_{\text{O}_2}^m}{D_{\text{O}_2}^m} \quad (18)$$

$D_{\text{O}_2}^m$ values for different temperatures and relative humidities were obtained from Sakai et al.'s work [44] and was fit to the following expression:

$$D_{\text{O}_2}^m = 9.78 \times 10^{-8} + 3.5 \times 10^{-9}T + 10^{-4}a_w \quad (19)$$

Fig. 7 shows the estimated peroxide rates at 75°C for Pt, PtCo and PtIrCo catalysts at the cathode-membrane interface when the local cathode potential is 0.6 V and the gas feed is pure oxygen at 1 atm. The peroxide formation rates at the alloy cathodes are higher (~ 3 – 4 times) than that of Pt at all humidities. The estimated rates are similar to those experimentally measured by Liu and Zuckerbrod [46]. The peroxide formation rate on Pt/Vulcan anode as a function of temperature and relative humidity is given in [2]. Estimated H_2O_2 formation rate on Pt/KB is lower than that on Pt/Vulcan. However, the estimated rates on both Pt/KB and Pt/Vulcan catalysts are lower than PtCo and PtIrCo catalysts supported on KB.

The potential profile across the membrane, measured in situ by Liu and Zuckerbrod [Fig. 17 in Ref. 46] and modeled by Burlatsky et al. [47] at open circuit conditions, indicate that the potential at the anode-membrane interface is $\sim 0 \text{ V}$. For the purpose of calculating H_2O_2 rates at the anode/membrane interface, a potential of $\sim 0 \text{ V}$ (i.e., $\eta = 0.695 \text{ V}$) was assumed to exist at the interface.

The oxygen flux across the membrane from the cathode to the anode is

$$F_{\text{O}_2} = \frac{D_{\text{O}_2}^m}{\delta} (C_{\text{O}_2}^c - C_{\text{O}_2}^a) \quad (20)$$

The concentration of oxygen at the anode-membrane interface approaches zero, since all of the oxygen crossing over the membrane to the anode side is reduced to water or reacts chemically with hydrogen.

$$R_{\text{H}_2\text{O}_2}^a = \chi_{\text{H}_2\text{O}_2} \frac{P_{\text{O}_2}^m}{\delta} \quad (21)$$

While the fraction of oxygen that is reduced to peroxide is a strong function of water activity, and is not a function of oxygen

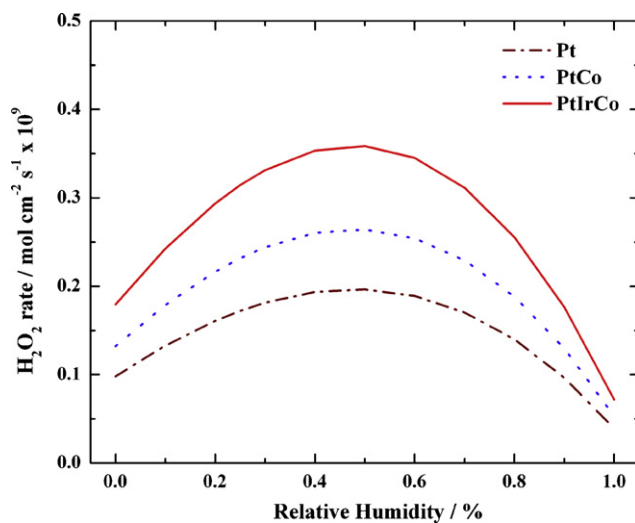


Fig. 8. Estimated rates of H_2O_2 formation/mol $\text{cm}^{-2} \text{s}^{-1}$ in the anode side of a PEM fuel cell for Pt (dash dot), PtCo (dot) and PtIrCo (line) catalysts as a function of relative humidity at 75°C . Local potential at the cathode was assumed to be $\sim 0 \text{ V}$ vs. SHE, which translates to an overpotential of 0.695 V for H_2O_2 formation.

concentration [Fig. 1c in Ref. 2]. An expression for $\chi_{\text{H}_2\text{O}_2}$ versus C_{H^+} was obtained from measured values at room temperature for Pt, PtCo and PtIrCo,

$$\chi_{\text{H}_2\text{O}_2}^{\text{Pt}} = 0.2081 - 0.1208(a_w) - 0.072(a_w)^2 - 2.132 \times 10^{-14}(a_w)^3 \quad (22)$$

$$\chi_{\text{H}_2\text{O}_2}^{\text{PtCo}} = 0.28 - 0.1625(a_w) - 0.0967(a_w)^2 \quad (23)$$

$$\chi_{\text{H}_2\text{O}_2}^{\text{PtIrCo}} = 0.38 - 0.2206(a_w) - 0.1313(a_w)^2 - 2 \times 10^{-14}(a_w)^3 \quad (24)$$

The estimated H_2O_2 formation rates at 75°C for Pt, PtCo and PtIrCo at the anode-membrane interface as a function of relative humidity are shown in Fig. 8. Again, the estimated peroxide formation rates are higher for PtCo and PtIrCo than Pt for all relative humidities. They go through a peak because oxygen permeability decreases with decreasing water activity whereas H_2O_2 selectivity increases with decrease in water activity. The estimated peroxide formation rates at 75°C , 1 atm and 94% RH conditions for other binary and ternary catalysts are tabulated in Table 1. The parameter values used in this study are tabulated in Table 2. For a complete description of peroxide formation rates on Pt as a function of humidity and temperature, see [2].

The estimated H_2O_2 formation rate on the cathode is higher than that of the anode by about three orders of magnitude. This is in accordance with the observations of Panchenko et al. [48,49] who used electron paramagnetic resonance spectroscopy to detect the presence of peroxide generated radicals. According to them, the radical centers produced at the cathode side of the PEM fuel cell causes membrane degradation. Further, they did not observe any membrane degradation on the anode side. Though the presence of radical species in the vicinity of the cathode had been identified via spectroscopic methods, their formation rates as well as their concentration distribution and half-lives have not been quantified yet.

Parasitic fuel loss due to H_2O_2 formation was estimated as a ratio of molar rates of H_2O_2 formation in the anode and the cathode (both Pt) to that of H_2 and O_2 respectively, in a fuel cell operating at 2 A cm^{-2} , 75°C and 94% RH fed with stoichiometric amounts of H_2 and O_2 . The percent fuel loss is shown in Fig. 9 for practical H_2O_2 selectivities. The loss of H_2 (due to reaction with O_2 from cathode forming H_2O_2) is less than a millionth of a percent while O_2 loss (due to reaction with protons forming H_2O_2) is less than a hundredth of

Table 2
Parameters used in the analysis of measured current at the Pt ring.^a

Parameters	Value	Comments
a	1	Measured, Ref. [2]
A	0.164025 cm^2	Ref. [16]
b	2	Measured, Ref. [2]
$C_{\text{O}_2}^*$	$1.274 \text{ mol cm}^{-3}$	Ref. [14] ^a
$D_{\text{O}_2}^*$	$2.2 \times 10^{-6} \text{ cm}^2 \text{ s}^{-1}$	Ref. [56]
E^0	0.695 V vs. SHE	–
EW	1100 g mol^{-1}	Ref. [57]
F	$96,485 \text{ C mol equiv.}^{-1}$	Ref. [58]
N	0.2	Measured
\bar{Q}	$210 \mu\text{C cm}^{-2}$ (real area)	Refs. [18,19]
R	$8.314 \text{ J mol}^{-1} \text{ K}^{-1}$	Ref. [58]
T^0	298 K	Measured
v	0.01 V s^{-1}	–
α	0.5	Assumed
δ_f	10^{-5} cm	Ref. [59]
ρ	1 g cm^{-3}	Ref. [58]
ν	$0.009 \text{ cm}^2 \text{ s}^{-1}$	Estimated
ω	2500 s^{-1}	Measured

^a The mole fraction solubility X_1 of oxygen in water is given as $\ln X_1 = A_2 + (B_2/T^*) + C_2 \ln T^*$, where $T^* = (T/100)\text{K}$. $A_2 = -66.7354$, $B_2 = 87.4755$ and $C_2 = 24.4526$.

a percent. Therefore, H_2O_2 selectivity as well as formation rates do not contribute to significant parasitic fuel loss.

4.3. Role of PtCo and PtIrCo on membrane degradation

Since the peroxide rates were higher for PtCo and PtIrCo than Pt and since these rates are higher at the cathode (O_2) than the anode (H_2), the effect of these catalysts on the membrane durability was tested on the oxygen side of a single-sided MEA with a built-in reference electrode. The reference electrode allowed specifying a potential on the cathode. In this circumstance, the reference electrode acted as the counter electrode as well. Fig. 10 shows fluorine emission rates (FER) from the single-sided MEA experiments where the working electrode was held at 600 mV versus H_2 on Au reference electrode. The MEA with Pt showed the highest FER of the three electrodes. The initial FER for the Pt electrode ($0.5 \mu\text{mol h}^{-1}$) is almost ten times higher than that of PtCo or PtIrCo electrodes. PtCo and PtIrCo electrodes have similar initial FER but PtCo shows

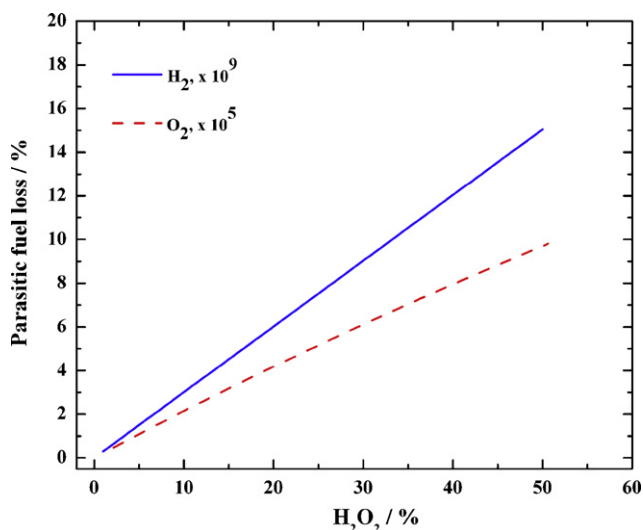


Fig. 9. Estimated parasitic fuel loss/% as a function of H_2O_2 selectivity on a catalyst in the anode (line) and the cathode (dash) of a fuel cell. The fuel loss was calculated at 75°C and 94% RH in a fuel cell operating at 2 A cm^{-2} with stoichiometric amounts of H_2 and O_2 while the local anode and cathode overpotentials are 0 and 0.6 V vs. SHE respectively.

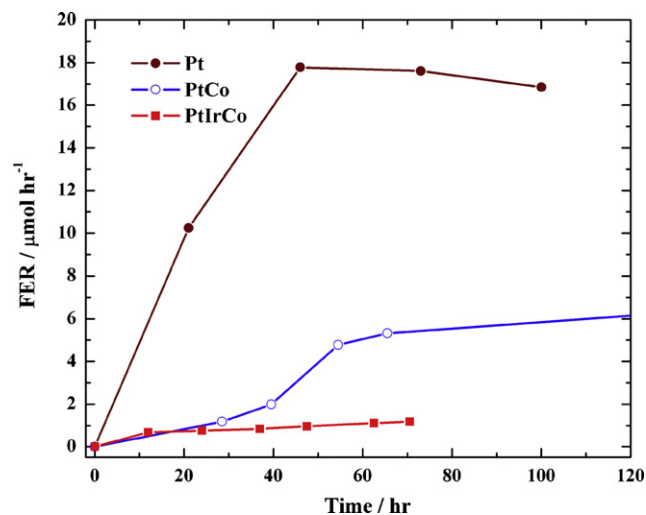


Fig. 10. Fluorine emission rates/ $\mu\text{mol h}^{-1}$ measured as a function of time from single-sided MEAs. The electrode with Pt (●), PtCo (○), and PtIrCo (■) was held at 600 mV vs. Au reference electrode throughout the test.

more FER after 25 h. Though Pt showed lower selectivity towards H_2O_2 formation than PtCo and PtIrCo catalysts, the MEA with Pt showed the most degradation. Similarly, MEA with the PtCo cathode showed higher degradation than that with the PtIrCo cathode. In effect, the catalyst with the highest peroxide selectivity and formation rates showed the least degradation rates and vice versa.

4.4. Stability of PtCo and PtIrCo

The above shown counter-intuitive result could be because of the extent of Pt and Co dissolution as Pt^{2+} and Co^{2+} and subsequent migration into the membrane, catalyzing membrane degradation reactions. To test this hypothesis, the stability of these catalysts was tested in a fuel cell via potential cycling between 0.87 and 1.05 V vs. SHE at 120°C in the absence of O_2 .

Fig. 11 shows the elemental map of Pt, Co and Ir for the three MEAs with Pt, PtCo and PtIrCo cathodes after potential cycling between 0.87 and 1.05 V vs. SHE at 120°C and 50% RH conditions. For elemental maps of MEAs before the potential cycling, see Fig. 8 of Yu et al. [50]. The cross-sections of the MEAs are shown with the cathode on the bottom. It is evident that the MEA with unalloyed Pt cathode shows the greatest concentration of Pt in the membrane among the three MEAs followed by those with PtCo and PtIrCo cathodes. Also, there is no evidence of Co or Ir in the membrane for the other two MEAs. The presence of elemental Pt at approximately one fifth of membrane thickness away from the cathode is due to the relative rates of diffusion between H_2 and O_2 (i.e., $D_{\text{H}_2}/D_{\text{O}_2} \cong 5$). The concentration of molecular H_2 and O_2 at this Pt plane tends to zero. The Pt^{2+} ions dissolving from the cathode tends to reduce to Pt above this plane (i.e., on the anode side) in the presence of H_2 ($\text{Pt}^{2+} + \text{H}_2 \rightarrow \text{Pt} + 2\text{H}^+$).

These results indicate that Pt alloy catalysts minimize membrane poisoning that might occur during load cycling in a fuel cell. Co dissolution, albeit to lesser extent than Pt, is also evident. In that there exists a thin layer of free Co particles in the membrane along the cathode-membrane interface in the Co map for the PtCo cathode. XRD results on the post-test MEAs (summarized in Table 3) showed significant sintering for the Pt cathode compared to PtCo and PtIrCo cathodes. For example, the Pt particle size increased from 3.3 nm to 6.1 nm for the Pt cathode. The particle size of PtIrCo changed from 5.9 nm to 6 nm with the final Pt particle size at 3.9 nm for the PtIrCo cathode. Phase separation was also observed during high temperature cycling. Post-test particle size analysis on the

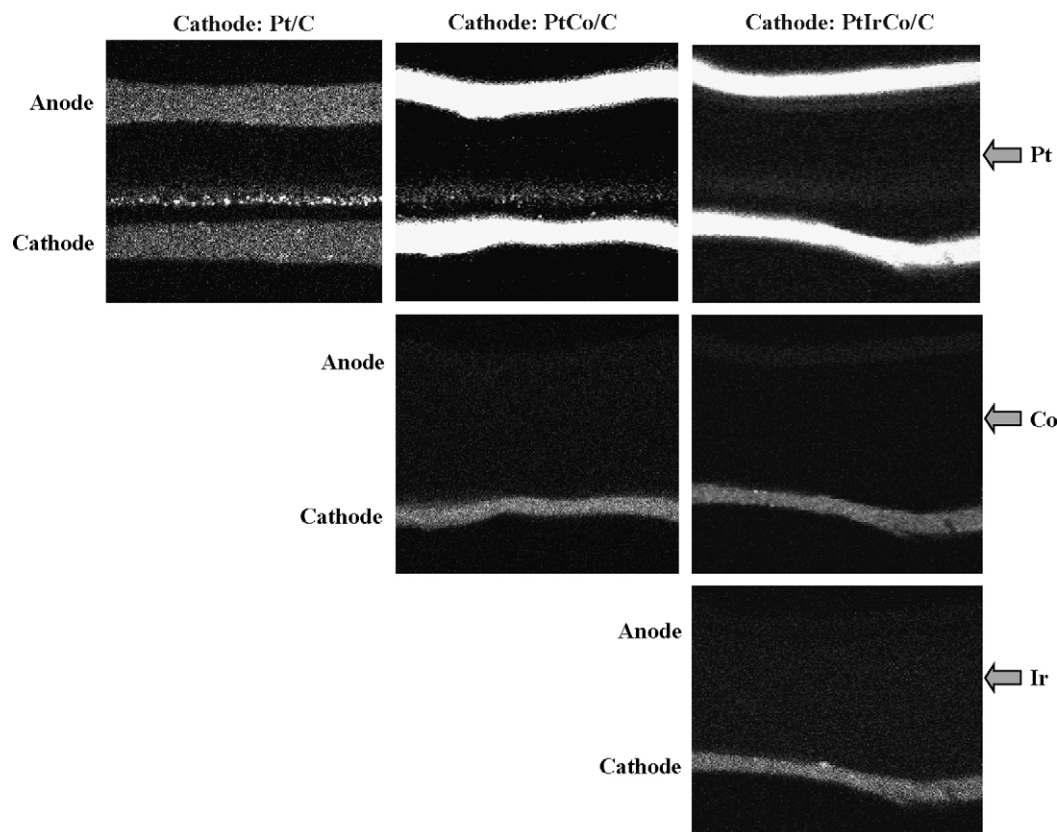


Fig. 11. Electron microprobe analysis (EPMA) for elemental Pt, Co and Ir from the MEAs after 2800 cycles on a fuel cell cathode between 0.87 and 1.05 V vs. SHE (1 min each) at 120 °C and 50% RH with H₂ on the anode and N₂ on the cathode.

anode catalyst layer indicates sintering as well. Though all three anodes had the same catalyst (Pt/KB), the extent of sintering was different during the course of the potential cycling test and was dependent on the nature of the cathode catalyst. As shown in the last column in Table 3, anode Pt sintering decreases from Pt to PtCo to PtIrCo. This is the first time this has been observed and needs further exploring. The current–voltage curves recorded with H₂/O₂ as well as with H₂/Air at 120 °C and 50% RH (not shown) at routine intervals during the potential cycling showed no performance degradation for the cell with PtIrCo cathode compared to PtCo and Pt cathodes. Table 3b summarizes relative cyclic stability, Pt concentration in the membrane, particle size change and the extent of sintering for these three catalysts. For example, cyclic stability

increases from Pt to PtCo to PtIrCo. For more on the performance and durability characteristics of PtIrCo catalysts, please see reports by Protsailo [51] and Haug et al. [52].

Fig. 12 shows the normalized cathode ECA loss during potential cycling in a fuel cell for these three catalysts. The trend seen here is qualitatively similar to that of the ECA loss seen after potential cycling experiment in the RDE cell. Pt cathode showed severe performance degradation with about 50% of its initial ECA lost after 2200 cycles. PtIrCo cathode showed very little degradation after similar number of cycles.

The apparent difference in the durability results (in terms of FER) in the single-sided MEA experiment between PtCo and PtIrCo electrodes is explained by a Fenton test with Co²⁺ as the Fenton ion.

Table 3

(a) Crystallite size of Pt, PtCo and PtIrCo catalysts before and after potential cycling tests at 65 °C and 120 °C and (b) relative performances of these catalysts during cycling tests.

(a)			
Catalyst	Initial size (Å)	2800 cycles 65 °C (Å)	2800 cycles 120 °C (Å)
Pt	33	45	61
PtCo	62	66	53 (Pt) 81 (PtCo)
PtIrCo	59	51	39 (Pt) 60 (PtIrCo)
(b)			
Catalyst	Pt	PtCo	PtIrCo
Cyclic stability		→	→
Pt concentration in membrane		←	←
Particle size	→	=	=
Extent of sintering		←	←

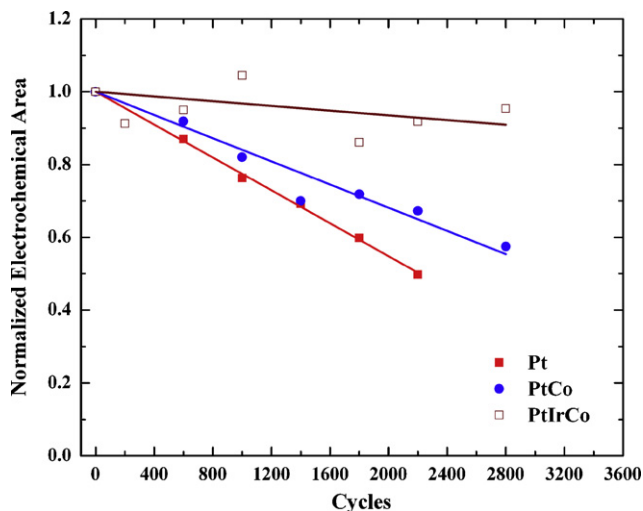


Fig. 12. Electrochemical area (normalized to its initial value) of the working electrode (Pt, PtCo, and PtIrCo supported on Ketjen Black) measured as a function of cycle number. The electrodes were cycled between 0.87 and 1.05 V vs. SHE (30 s at each potential) at 50% RH in a fuel cell and 120 °C. The total metal loadings were similar.

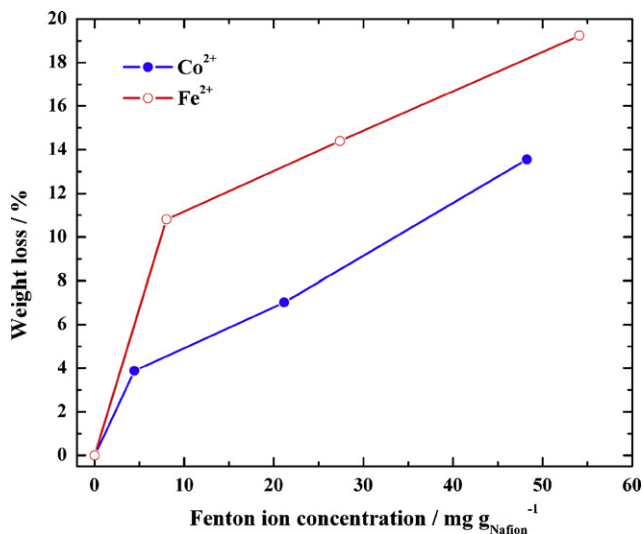


Fig. 13. Weight loss (%) observed on Nafion® 111 membrane samples (2 in. × 2 in.) after 96 h of Fenton testing for various concentrations of Fenton ions (Co²⁺ and Fe²⁺). Cobalt nitrate [Co(NO₃)₂·6H₂O] and iron sulfate (FeSO₄·6H₂O) were respectively used to impregnate Co²⁺ and Fe²⁺ into Nafion membrane.

Fig. 13 shows the observed weight loss from a Nafion® 111 membrane as a function of Fenton ion concentration for Fe²⁺ and Co²⁺ ions. It is readily perceivable that the presence of Co²⁺ does degrade the membrane akin to Fe²⁺, the well-known Fenton ion. Fenton test with Ir³⁺ as Fenton ion was not carried out because of the absence of iridium ions in the membrane even in the vicinity of the cathode catalyst-membrane interface as seen in the post cycling EPMA results. It should also be noted that results from a Fenton test alone does not dictate membrane durability under fuel cell conditions [53].

4.5. Implications

These results have implications on catalyst synthesis as well as on the operational aspects of a PEM fuel cell. H₂O₂ selectivity, on fuel cell catalysts (especially for cathodes) will now become less important compared to their stability. Consideration should be

given if the H₂O₂ selectivity is abnormally high. For example, H₂O₂ selectivity of 100% will totally shut off the cathode reaction. Though the parasitic fuel loss for such high selectivity would be very small, the parasitic power loss would be 100%.

From a functional standpoint, this also impacts the practice of using air-bleed technique [54] (i.e., adding a small quantity of O₂ with the H₂ fuel) as a way to mitigate CO poisoning in the PEMFC anode. The current understanding is that air-bleed, in addition to CO oxidation, contributes to H₂O₂ formation in the anode and thus to membrane degradation [55]. This may not be true if the catalysts are more stable.

5. Conclusions

Binary and ternary Pt alloys supported on high surface area carbon were shown to have higher selectivity towards hydrogen peroxide formation in the ORR than unalloyed Pt. Though this higher selectivity meant higher peroxide formation rates in a functional fuel cell, the durability experiments indicated that MEAs with binary and ternary Pt catalysts had lower fluorine emission rates than those with just Pt, indicative that MEAs with alloys catalysts are more durable. This was because unalloyed Pt showed higher dissolution rates than binary and ternary Pt catalysts, which meant higher migration flux of Pt²⁺ ions into the membrane. The presence of metal ions in the membrane in conjunction with the availability of gaseous H₂ and O₂ as well as peroxy and hydroperoxy radicals dictate membrane durability. Therefore, peroxide formation rates alone do not dictate the durability of an MEA. Further, based on estimated peroxide formation rates in an anode and a cathode of a functional fuel cell, the parasitic fuel loss was shown to be less than a millionth of a percent for H₂ and less than a thousandth of a percent for O₂ for practical H₂O₂ selectivities. Therefore, it is concluded that H₂O₂ selectivity and formation rates in fuel cell catalysts may not be as important as previously thought on both durability and parasitic fuel loss standpoints. We recommend based on these studies that mass activity and stability (i.e., low catalyst dissolution) be given more importance than H₂O₂ selectivity during the process of fuel cell catalyst design and characterization.

Acknowledgements

The US Department of Energy supported this work under contract number DOE-DE-FC36-02AL, for which the authors are grateful. The authors thank Michael E. Fortin for oxygen permeability measurements and Shruti Modi for guidance on Fenton tests.

Appendix A. Nomenclature

<i>a</i>	reaction-order with respect to O ₂ in the H ₂ O ₂ formation reaction
<i>a_w</i>	water activity
<i>A</i>	disk area (cm ²)
<i>b</i>	reaction-order with respect to H ⁺ in the H ₂ O ₂ formation reaction
<i>C_{H+}</i>	proton concentration (mol cm ⁻³)
<i>C_{H2O}</i>	water concentration in the membrane (mol cm ⁻³)
<i>C_{O2}</i> [*]	oxygen concentration in the bulk of the electrolyte (mol cm ⁻³)
<i>C_{O2}</i> ^f	oxygen concentration in Nafion® film (mol cm ⁻³)
<i>C_{O2}</i> ^a	oxygen concentration in Nafion® 112 membrane-anode catalyst layer interface (mol cm ⁻³)
<i>C_{O2}</i> ^c	oxygen concentration in Nafion® 112 membrane-cathode catalyst layer interface (mol cm ⁻³)

$D_{O_2}^*$	oxygen diffusion coefficient in the electrolyte ($\text{cm}^2 \text{s}^{-1}$)
$D_{O_2}^f$	oxygen diffusion coefficient in Nafion [®] film ($\text{cm}^2 \text{s}^{-1}$)
$D_{O_2}^m$	diffusion coefficient of O_2 in Nafion [®] 112 membrane ($\text{cm}^2 \text{s}^{-1}$)
E°	equilibrium potential (0.695 V vs. SHE at 25 °C and 101 kPa)
E_a^*	activation energy for H_2O_2 formation (J mol^{-1})
E_{app}	applied potential (V vs. SHE)
EW	equivalent weight of Nafion [®] polymer (1100 g equiv. ⁻¹)
F	Faraday constant (96,485 C mol ⁻¹)
I	current density (A cm^{-2})
I_{ring}	ring current (mA)
I_{disk}	disk current (mA)
j	total peroxide current density (mA cm^{-2})
j_{disk}	disk current density (mA cm^{-2})
j_D	diffusion-limited current density (mA cm^{-2})
j_{kin}	kinetic current density (mA cm^{-2})
k_b	rate constant for H_2O_2 electro-oxidation (s^{-1})
k_f	rate constant for H_2O_2 formation ($\text{mol}^2 \text{cm}^{-5} \text{s}^{-1}$)
N	collection efficiency
n	number of electrons transferred per O_2 molecule in H_2O_2 formation (2)
$P_{O_2}^m$	permeability of O_2 in Nafion [®] 112 membrane ($\text{mol cm}^{-1} \text{s}^{-1}$)
Q	charge density (C cm^{-2}) (geometric area)
\bar{Q}	charge density of Pt (C cm^{-2}) (geometric area)
R	universal gas constant (8.314 J mol ⁻¹ K ⁻¹)
T	temperature (K)
t	time (s)
V	potential (V vs. SHE)
ν	scan rate (V s^{-1})
W	catalyst loading ($\text{mg}_{Pt} \text{cm}^{-2}$) (geometric area)

Greek

α	transfer coefficient
δ	Pt/C electrode thickness (cm)
δ_f	Nafion [®] film thickness (cm)
ρ	density of Nafion [®] (g cm^{-3})
ν	kinematic viscosity ($\text{cm}^2 \text{s}^{-1}$)
η	overpotential (V vs. SHE)
λ	moles of water per sulfonic acid group in Nafion [®]
$\chi_{H_2O_2}$	fraction of O_2 reducing to H_2O_2
ω	electrode rotation rate (s^{-1})

Superscript

0	standard state or equilibrium
a	anode
c	cathode

Subscript

ad	adsorbed
b	backward reaction, bulk
D	diffusion
disk	Pt/Nafion [®] coated disc electrode
f	Nafion [®] film or forward reaction
kin	kinetic
ring	Pt ring electrode

References

- [1] E. Yeager, *Electrochim. Acta* 29 (1984) 1527.
- [2] V.A. Sethuraman, J.W. Weidner, A.T. Haug, S. Motupally, L.V. Protsailo, *J. Electrochem. Soc.* 155 (2008) B50.
- [3] A. Bosnjakovic, S. Schlick, *J. Phys. Chem. B* 108 (2004) 4332.
- [4] M. Inaba, T. Kinumoto, M. Kiriake, R. Umeybayashi, A. Tasaka, Z. Ogumi, *Electrochim. Acta* 51 (2006) 5746.
- [5] M. Inaba, H. Yamada, R. Umeybayashi, M. Sugishita, A. Tasaka, *Electrochemistry* 75 (2007) 207.
- [6] T. Kinumoto, M. Inaba, Y. Nakayama, K. Ogata, R. Umeybayashi, A. Tasaka, Y. Iriyama, T. Abe, Z. Ogumi, *J. Power Sources* 158 (2006) 1222.
- [7] D.A. Schiraldi, *J. Macromol. Sci. C: Polymer Rev.* 46 (2006) 315.
- [8] US Patents 5,013,618 (1991); 4,880,711 (1989); 4,447,506 (1984).
- [9] US Patents 5,189,005 (1993); 5,593,934 (1997).
- [10] T.J. Schmidt, H.A. Gasteiger, G.D. Stäb, P.M. Urban, D.M. Kolb, R.J. Behm, *J. Electrochem. Soc.* 145 (1998) 2354.
- [11] T.J. Schmidt, U.A. Paulus, H.A. Gasteiger, R.J. Behm, *J. Electroanal. Chem.* 508 (2002) 41.
- [12] N. Markovic, P.N. Ross, *J. Electroanal. Chem.* 330 (1992) 499.
- [13] V. Stamenkovic, N.M. Markovic, P.N. Ross Jr., *J. Electroanal. Chem.* 500 (2001) 44.
- [14] L.H. Gevantman, in: D.R. Lide (Ed.), *CRC Handbook of Chemistry and Physics*, 79th ed., CRC Press, New York, 1998–1999, p. 8.
- [15] W.J. Albery, M.L. Hitchman, *Ring-Disc Electrodes*, Clarendon Press, Oxford, 1971.
- [16] *Rotated Ring-Disc Electrodes: DT21 Series*, Pine Instrument Company, Raleigh, NC 27617.
- [17] S. Trasatti, O.A. Petrii, *Pure Appl. Chem.* 63 (1991) 711.
- [18] T. Biegler, D.A.J. Rand, R. Woods, *J. Electroanal. Chem.* 29 (1971) 269.
- [19] J. Bett, K. Kinoshita, K. Routsis, P. Stonehart, *J. Catal.* 29 (1973) 160.
- [20] V. Mittal, H.R. Kunz, J.M. Fenton, Abstract #1192, in: 208th Meeting of the Electrochemical Society, Los Angeles, CA, October 16, 2005.
- [21] V.O. Mittal, H.R. Kunz, J.M. Fenton, *Electrochem. Solid State Lett.* 9 (2006) A299.
- [22] V.O. Mittal, H.R. Kunz, J.M. Fenton, *J. Electrochem. Soc.* 153 (2006) A1755.
- [23] V.O. Mittal, H.R. Kunz, J.M. Fenton, *J. Electrochem. Soc.* 154 (2007) B652.
- [24] M.R. Tarasevich, A. Sadkowsky, E. Yeager, in: J.O'M. Bockris, B.E. Conway, E. Yeager, S.U.M. Khan, R.E. White (Eds.), *Comprehensive Treatise in Electrochemistry*, Plenum Press, New York, 1983 (Chapter 6).
- [25] S.K. Zečević, J.S. Wainright, M.H. Litt, S.L.J. Gojković, R.F. Savinell, *J. Electrochem. Soc.* 144 (1997) 2973.
- [26] A. Damjanovic, G. Hudson, *J. Electrochem. Soc.* 135 (1988) 2269.
- [27] U.A. Paulus, A. Wokaun, G.G. Scherer, T.J. Schmidt, V. Stamenkovic, V. Radmilovic, N.M. Markovic, P.N. Ross, *J. Phys. Chem. B* 106 (2002) 4181.
- [28] K.C. Neyerlin, W. Gu, J. Jorne, H.A. Gasteiger, *J. Electrochem. Soc.* 153 (2006) A1955.
- [29] A.J. Bard, L.R. Faulkner, *Electrochemical Methods*, Wiley & Sons, Inc., New York, 1980.
- [30] A.B. Anderson, T.V. Albu, *J. Electrochem. Soc.* 147 (2000) 4229.
- [31] R.A. Sidik, A.B. Anderson, *J. Electroanal. Chem.* 528 (2002) 69.
- [32] Y. Wang, P.B. Balbuena, *J. Chem. Theory Comput.* 1 (2005) 935.
- [33] V. Stamenkovic, B.N. Grgur, P.N. Ross, N.M. Markovic, *J. Electrochem. Soc.* 152 (2005) A277.
- [34] N.A. Anastasijevic, Z.M. Dimitrijevic, R.R. Adzic, *Electrochim. Acta* 31 (1986) 1125.
- [35] D.R. Morris, X. Sun, *J. Appl. Polym. Sci.* 50 (1993) 1445.
- [36] D. Rivin, C.E. Kendrick, P.W. Gibson, N.S. Schneider, *Polymer* 42 (2001) 623.
- [37] N.H. Jalani, P. Choi, R. Datta, *J. Membrane Sci.* 254 (2005) 31.
- [38] T. Zawodzinski, M. Neeman, L. Sillerud, S. Gottesfeld, *J. Phys. Chem.* 95 (1991) 6040.
- [39] J.T. Hinatsu, M. Mizuhata, H. Takenaka, *J. Electrochem. Soc.* 141 (1994) 1493.
- [40] L.M. Onishi, J.M. Prausnitz, J. Newman, *J. Phys. Chem. B* 111 (2007) 10166.
- [41] S. Motupally, A.J. Becker, J.W. Weidner, *J. Electrochem. Soc.* 147 (2000) 3171.
- [42] T. Fuller, Ph.D. Dissertation, University of California, Berkeley, 1989.
- [43] R.C. Reid, J.M. Prausnitz, T.K. Sherwood, *The Properties of Gases and Liquids*, McGraw Hill Inc., New York, 1977.
- [44] T. Sakai, H. Takenaka, E. Torikai, *J. Electrochem. Soc.* 133 (1986) 88.
- [45] K. Broka, P. Ekdunge, *J. Appl. Electrochem.* 27 (1997) 117.
- [46] W. Liu, D. Zukerbrod, *J. Electrochem. Soc.* 152 (2005) A1165.
- [47] S. Burlatsky, T. Jarvi, V. Atrazhev, Abstract # 502, The Electrochemical Society Meeting Abstracts, Volume 2005–2, Los Angeles, CA, October 16–21, 2005.
- [48] A. Panchenko, H. Dilger, J. Kerres, M. Hein, A. Ullrich, T. Kaz, E. Roduner, *Phys. Chem. Chem. Phys.* 6 (2004) 2891.
- [49] A. Panchenko, Dipl.-Chem., Institut für Physikalische Chemie der Universität Stuttgart, October 2004.
- [50] P. Yu, M. Pemberton, P. Plasse, *J. Power Sources* 144 (2005) 11.
- [51] L. Protsailo, Development of High Temperature Membranes and Improved Cathode Catalysts, United States Department of Energy Report, December 2005.
- [52] A.T. Haug, L.V. Protsailo, S. Modi, V.A. Sethuraman, S. Motupally, Characterization of membranes and catalysts for high temperature PEM fuel cells, United States Department of Energy–High Temperature Working Group, in: 208th Meeting of the Electrochemical Society, Los Angeles, CA, October 20, 2005.
- [53] V.A. Sethuraman, J.W. Weidner, A.T. Haug, L.V. Protsailo, *J. Electrochem. Soc.* 155 (2008) B119.
- [54] Z. Jusys, R.J. Behm, *J. Phys. Chem. B* 108 (2004) 7893.
- [55] M. Inaba, M. Sugishita, J. Wada, K. Matsuzawa, H. Yamada, A. Tasaka, *J. Power Sources* 178 (2008) 699.
- [56] Q. Guo, V.A. Sethuraman, R.E. White, *J. Electrochem. Soc.* 151 (2004) A983.
- [57] K.A. Mauritz, R.B. Moore, *Chem. Rev.* 104 (2004) 4535.
- [58] R.H. Perry, D.W. Green, *Perry's Chemical Engineer's Handbook*, 7th ed., McGraw Hill, 1997.
- [59] U.A. Paulus, T.J. Schmidt, H.A. Gasteiger, R.J. Behm, *J. Electroanal. Chem.* 495 (2001) 134.